AR-009-759

DSTO-TN-0046

A Validated Finite Element Model of an F-111 Lower Wing Skin Structural Detail at Forward Auxillary Spar Station (FASS) 281.28

D. Keeley, R. Callinan and S. Sanderson

APPROVED FOR PUBLIC RELEASE

19970429 161

DEPARTMENT OF DEFENCE

DEFENCE SCIENCE AND TECHNOLOGY ORGANISATION

A Validated Finite Element Model of an F-111 Lower Wing Skin Structural Detail at Forward Auxiliary Spar Station (FASS) 281.28

D. Keeley, R. Callinan and S. Sanderson

Airframes and Engines Division
Aeronautical and Maritime Research Laboratory

ABSTRACT

This report describes an AMRL developed and validated Finite Element (FE) model of the F-111A lower wing skin (Serial Number A-10-824) at Forward Auxiliary Spar Station (FASS) 281.28 and constitutes part of an extensive AMRL bonded composite repair substantiation program initiated by the RAAF following the discovery of fatigue cracking at FASS 281.28 in an F-111C aircraft. Strain data from the FE model is compared with measured strain gauge data from an F-111A static test wing under Cold Proof Loading Test (CPLT) or limit conditions. A relationship between nominal section stress at FASS 281.28 and local bending moment is established. The FE model will be further developed to include the fatigue crack, the adhesive and the boron epoxy patch.

RELEASE LIMITATION

Approved for public release

D E P A R T M E N T   O F   D E F E N C E

———————————◆———————————

DEFENCE SCIENCE AND TECHNOLOGY ORGANISATION

APPROVED FOR PUBLIC RELEASE

A Validated Finite Element Model of an F-111 Lower Wing Skin Structural Detail at Forward Auxillary Spar Station (FASS) 281.28

Executive Summary

This report documents the development and validation of a three-dimensional Finite Element (FE) model of the F-111 lower wing skin at a structural detail in the skin approximately midway between the inboard and outboard fixed pylons. This work forms part of a comprehensive repair substantiation package for a bonded composite repair to cracking at that location on a particular RAAF F-111C aircraft, Tail Number A8-145. By correlating the FE strain results with experimental strain gauge data obtained from a static test on a full-scale wing, a reliable and accurate relation between the nominal stress at the cracking location and the wing pivot bending moment can be determined. This "stress equation" is of fundamental importance in specifying the stresses to be applied during structural testing of representative specimens as part of the repair substantiation. The baseline FE model will also then be modified to include the crack and the patch repair.

Contents

Notation

$\bar{z}$	Neutral axis location of wing skin
C	Strain shift in NASCE
E	Youngs Modulus
ε_x	Strain in x direction (spanwise)
fe_{actual}	Actual FE measured strain data
F_H	Applied force at jack H
F_I	Applied force at jack I
m	gradient of NASCE
M_{281}	Local bending moment at FASS 281.28
σ	stress
σ_N	Nominal stress for the fuel-flow hole at FASS 281.28
v	Poisson's ratio
y	chord-wise direction

List of abbreviations

AMRL	Aeronautical and Maritime Research Laboratory
CPLT	Cold Proof Load Test
FAS	Forward Auxiliary Spar
FASS	Forward Auxiliary Spar Station
FE	Finite element
FFP	Fuel-Flow Passage
NASCE	Neutral Axis Strain Correction Equation
RAAF	Royal Australian Air force
USAF	United States Air Force

1. Introduction

In February 1994, a 48 mm chord-wise fatigue crack was detected at a Fuel-Flow Passage (FFP) at Forward Auxiliary Spar Station (FASS) 281.28 in the lower wing skin of a RAAF F-111C aircraft (Tail Number A8-145). The location of the crack is shown below in Figure 1. This cracking led to the development and interim approval by the RAAF of an adhesively bonded boron epoxy patch repair subject to a detailed repair substantiation to be undertaken by AMRL. As part of this substantiation, a Finite Element (FE) model of the fuel-flow passage and surrounding wing area was produced. The model has been calibrated against strain survey data from a full scale test wing. This model allows an accurate evaluation of the stress distribution at FASS 281.28. This model is envisaged to become the base for later modifications. These modifications will allow the investigation of a variety of crack lengths, wing skin thicknesses and bonded boron composite patch configurations.

The basic model will also be extended to represent full scale "panel" and "box" specimens. These specimens will be used in static and fatigue testing. To validate the loads applied in specimen testing, an accurate measure of far-field stress under known load conditions must be determined. This applied stress is determined from the validation process of the finite element model of the wing skin at Cold Proof Load Test (CPLT) conditions.

This report assesses the validity and limitations of the base wing skin model and documents the calculation of the far-field stress under known CPLT loading.
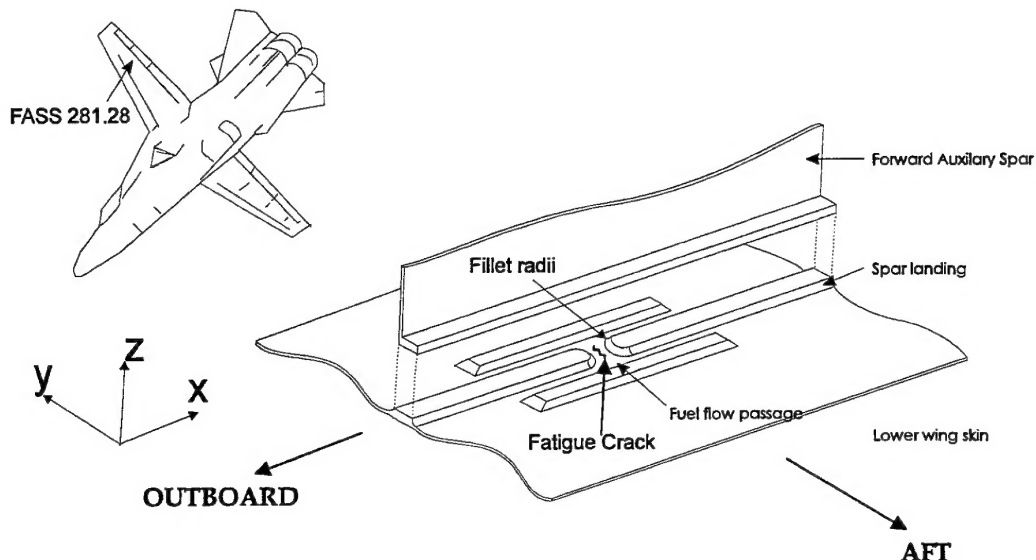

Fig 1. Fuel-flow passage

2. Test wing

2.1 History

The FE model was compared to the results from a strain survey [1] performed on the right wing of an F-111A (wing serial number A-10-824) supplied to AMRL by the USAF. The F-111C wing is 42 inches longer than the F-111A wing due to a wing tip extension. The wing box structure is however identical. The strain survey from [1] demonstrated that the strain distribution at FASS 281.28 is a function of local bending moment only. The F-111A test wing was therefore acceptable to obtain the local strain distribution at FASS 281.28.

The service history of the test wing prior to arriving at AMRL is largely unknown. The service life (approximately 20 years) suggests at least three to four thousand flying hours. In addition, the wing has undergone a CPLT cycle prior to service release to the USAF, and based upon service life, at least one other CPLT since. F-111 wings undergo CPLT testing at certain stages throughout their service life. Presently, in service F-111 wings are nearing their fourth CPLT. The application of CPLT cycles to the wing is important because it will be shown later that the CPLT applies sufficiently high loads to induce significant yielding in the FASS 281.28 region.

2.2 Manufacture

After cold forming, the F-111 wing skins are chemically milled to produce the integral stiffeners. Once completed, ultrasound tests are used to determine if the skin thickness falls within design tolerances. The skins are then rough sawed and machine finished with portable hand routers [2].

2.3 Geometry

2.3.1 Accuracy

Due to the low thicknesses and high expected loading, small changes in wing skin geometry can have a relatively large effect on the stress distributions [3]. To allow an optimum correlation between the strain gauge results and the finite element model, the geometry of the finite element model must match that of the actual wing skin as closely as possible.

Design tolerances allow a minimum five per cent deviation from the design specifications for manufacturing purposes. In addition the use of hand-routing can lead to a non-uniform surface thickness. These factors can affect the accuracy of the FE

model. To minimise run times and thickness measurements, the average thickness of the test wing skin at FASS 281.28 was used as a representative FE model wing skin thickness.

2.3.2 Wing skin thickness

Ultrasonic thickness measurements on the test wing at FASS 281.28 were undertaken [4] over a rectangular area (48 mm x 60 mm) as indicated by Figure 2. These measurements were taken at a spacing of 3 mm in both directions, and are expected to be accurate to within ±0.1 mm.
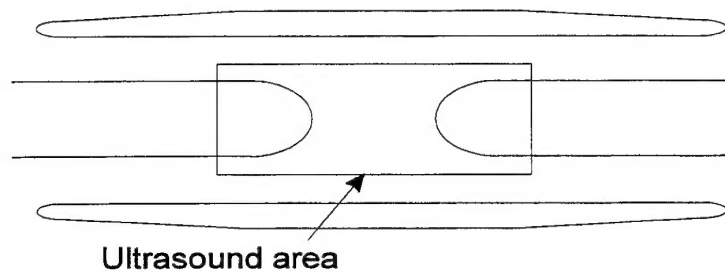

Ultrasound area

Fig 2. Location of ultrasound testing region at FASS 281.28.

Figures 3 & 4 show surface plots of scanned region. Several limitations apply to the ultrasound results. Ultrasound testing relies upon flat surfaces to successfully rebound the thickness measurement signals, therefore fillet radii cannot be obtained from the test. The inside surface of the wing skin has a thin layer of paint approximately 5×10^{-2} mm thick over the tested surface. This extra thickness can result in as a much as a 0.1 mm difference between the ultrasound readings and the actual wing skin thickness.
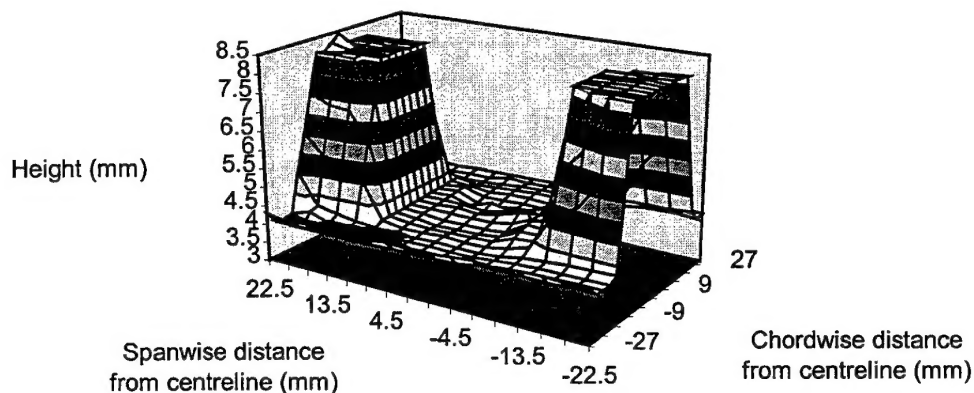

Fig 3. Ultrasound thickness measurements surrounding FASS 281.28

3

All dimensions measured in millimetres
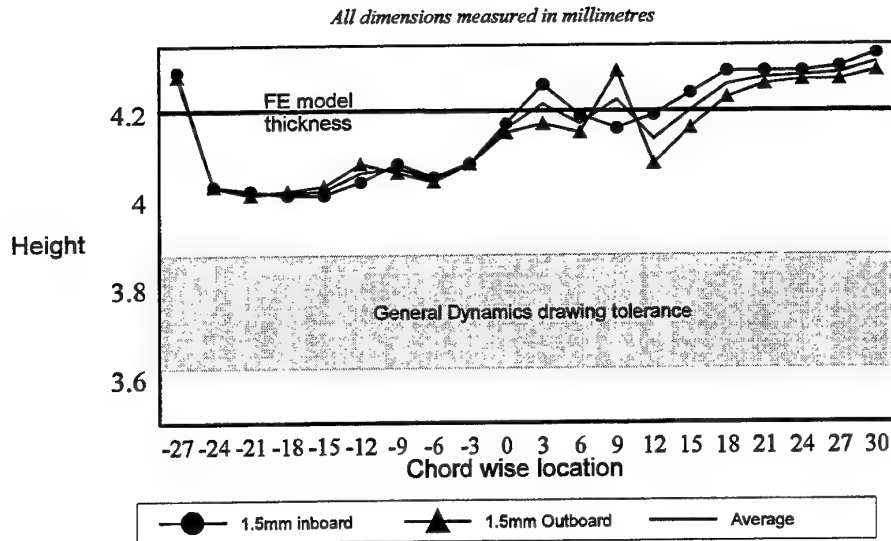
Fig 4. *Ultrasound thickness measurements along centre of fuel-flow passage*

2.3.3 Fillet Radii

A polyether mould of that region was created to obtain an accurate measurement of the fillet radii at the spar landing step down, as shown in Figure 5. The mould was fabricated by wet casting and in-situ curing [5]. After the mould was removed and dissected, radii measurements with circle templates were taken. Allowing for possible shrinkage of the mould, the radius of the spar landing step down was approximated to be between eight and ten millimetres.
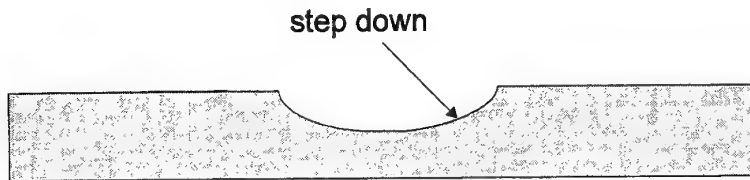
Fig 5. Location of spar landing step down on the fuel-flow passage

3. Strain Survey

3.1 Location

A strain survey under CPLT simulated loading was performed at FASS 281.28 on the outer wing skin surface of the test wing as documented in detail in [1]. Both uniaxial strip gauges (KFC-1-D19-23) and rosette gauges (FRA-6-23) were used, as indicated in Figure 6. The elements in the strip gauges were oriented in the span-wise direction.

Fig 6. *Location of strain gauges at FASS 281.28 on the outer wing skin.*

3.2 Loading

The wing was loaded according to the cold proof load test configuration outlined in [6]. Loading jacks were applied at points shown by Figure 7.

Inches from pivot 0.26 chord line
(mm from pivot along 0.26 chord line)

248.1 (6302)

300.0 (7620)

7.8 (198)   H

6.0 (152)   I
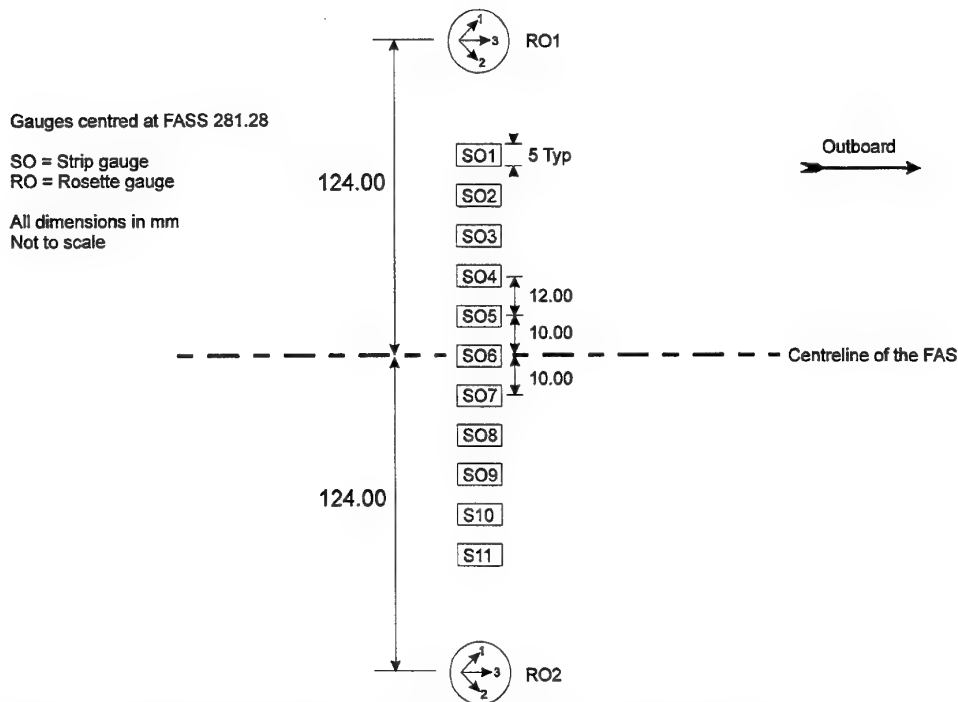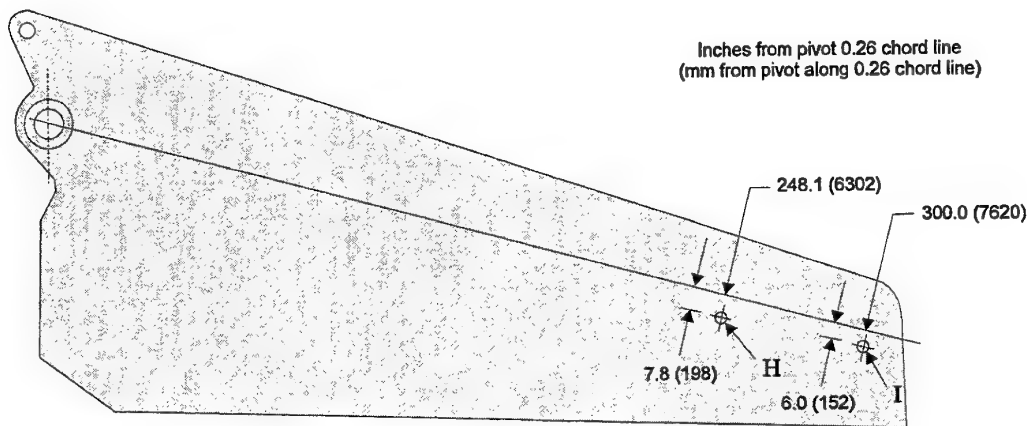
Fig 7. Location of wing jacks on the outer wing skin

3.3 Estimates of Nominal Stress at FASS 281

The applied wing jack loads at CPLT loading are:

F_H = 29 200 lbs (130 kN)
F_I = 4 900 lbs (22 kN).

From these loads, the ratio of local nominal skin stress at FASS 281 ($\sigma_{FASS\ 281}$)to local bending moment ($BM_{FASS281}$) can be established. This is based on the original stress analysis for the wing box [6]. The calculations are detailed in Appendix A and the resulting ratio is as follows:

$\sigma_{FASS\ 281}/ BM_{FASS\ 281} = 0.0189\ in^{-3}$

Using this relationship and the known local bending moment under CPLT loading, the stress at FASS 281 under CPLT conditions can be estimated (Appendix A) as follows:

$\sigma_{FASS\ 281} = 30400\ psi$

This has been based on the original stress analysis for the wing box structure. It can also be determined from the strain survey results [1]. Under CPLT loading, the nominal strain at FASS 281 can be estimated by averaging the strain at rosettes RO1 and RO2 (element 3 only, refer to Figure 6) and converting this to a stress as follows:

Strain average:

$$\frac{2851+2486}{2} = 2669 \ \mu\varepsilon$$

$\sigma = E.\varepsilon$

$\quad = 72\ 397 \times 2669$

$\quad = 193.2\ \text{MPa} \ (28000\ \text{psi})$

Therefore the local stress to bending moment ratio becomes:

$\sigma_{\text{FASS 281}}/\ BM_{\text{FASS 281}} = 0.0174\ \text{in}^{-3}$

The local stress to bending moment ratio based upon the strain survey results as described above must be validated by the FE model. This is achieved by applying a loading of 28 000 psi (193 MPa) to the model and evaluating the full strain distribution against the strain survey results (see section 4).

4. Finite element model

4.1 General Description

The FE wing-skin model was produced using PAFEC version 8.1. Reference [7.] contains working level details of the development of the model. This includes references to the location of the input and output files which relate to the results presented in this report. The model consists of both one-dimensional gap elements and three dimensional quadrilateral and triangular elements. It is loaded in span-wise tension (X direction).
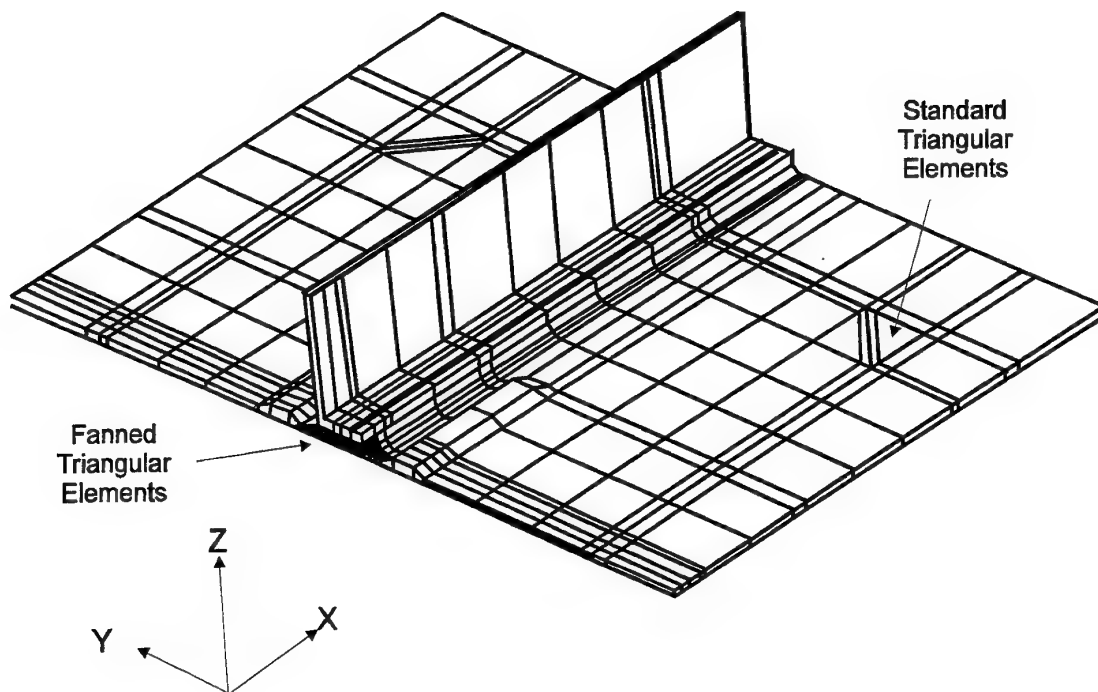
Fig 8. Finite element model of wing skin

4.2 Assumptions

The model was assumed to be linearly elastic and symmetrical about a chord-wise axis through the centre of the fuel-flow passage (Figure 8). The assumed radii in the critical area are shown in Figure 9. The restraints and loading are shown in Figure 11 and 12 respectively.

4.3 Material properties

The wing skin was manufactured from aircraft grade aluminium 2024-T851. Material properties used were based upon the Mil-hdbk values for a quarter inch thick plate [8].
E= 72.395 GPa (10.5 E+06 psi) $v= 0.33$

4.4 Geometry

The geometry of the wing skin in the FE model, shown below in Figure 9, was calculated using a FORTRAN program [9]. This program allows the thicknesses and radii of the model to be changed with minimum reprogramming. A representative

wing skin thickness of 4.19 mm and a spar landing thickness of 8.19 mm were selected based upon the ultrasonic measurements (section 2.3.2). The fillet radii at the fuel-flow hole region was based upon the mould measurements and General Dynamics drawing specifications [10]. A half spar was modelled to give the spar landing the correct out of plane support.
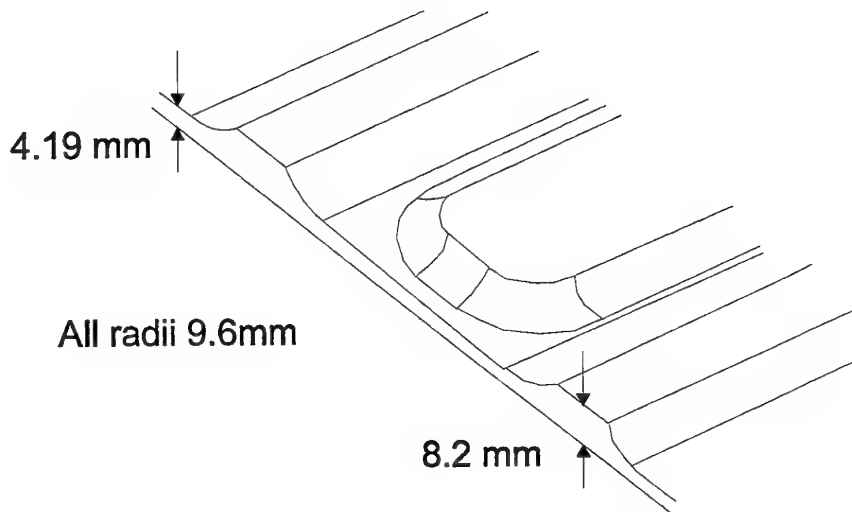

Fig 9. Geometry surrounding the fuel-flow passage

4.5 Elements

The finite element model consisted of three-dimensional twenty noded quadrilateral elements and a small region of sixteen noded triangular prism elements. Gap elements between the spar and spar landing were used.

4.5.1 Triangular elements

Triangular elements were located at two regions, near the fuel-flow passage (fanned elements) and at the far corners of the envisaged boron patch location (standard elements), shown in Figure 8. The fanned elements allowed a simple transition into a mesh that could later be used for the implementation of crack tip elements. The standard elements allowed for a simple and accurate modelling of the patch corners.

4.5.2 Gap elements

The wing skin spar cap is attached to the spar with interference fit taper lok fasteners. Gap elements were used to model the correct spar to skin connectivity. The effective bolt area was modelled as shown in Figure 10 below. Gap elements were placed between the remaining surface of the spar landing and the adjoining surface of the

spar cap. In addition to allowing a less rigid joining of the spar, these elements prevent the spar from deforming through the spar landing.
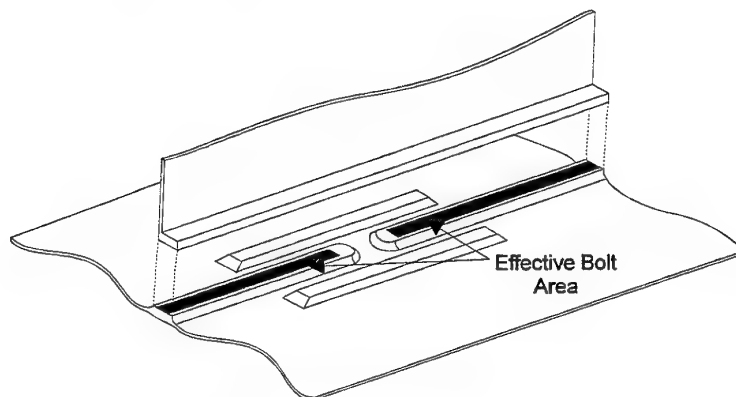
Fig 10. Location of effective bolt area

4.6 Restraints

A surface restraint to model symmetry was placed in the span-wise direction along the chord-wise symmetry axis as shown in Figure 11. A line of vertical restraint along the top surface of the spar was used to approximate the restraint transferred through the test wing spar. Similarly, lines of out-of-plane vertical restraints were placed along the spanwise side edges and the far-field chord-wise edge of the model. These restraints approximate the effect of the side spars and transverse members in the wing. To statically position the model, single restraint in the transverse (chord-wise) direction was placed as shown.

Lines of
vertical restraints

Faces restrained in the
spanwise direction
(due to symmetry)

Chordwise   Spanwise

Single noded
chordwise restraint
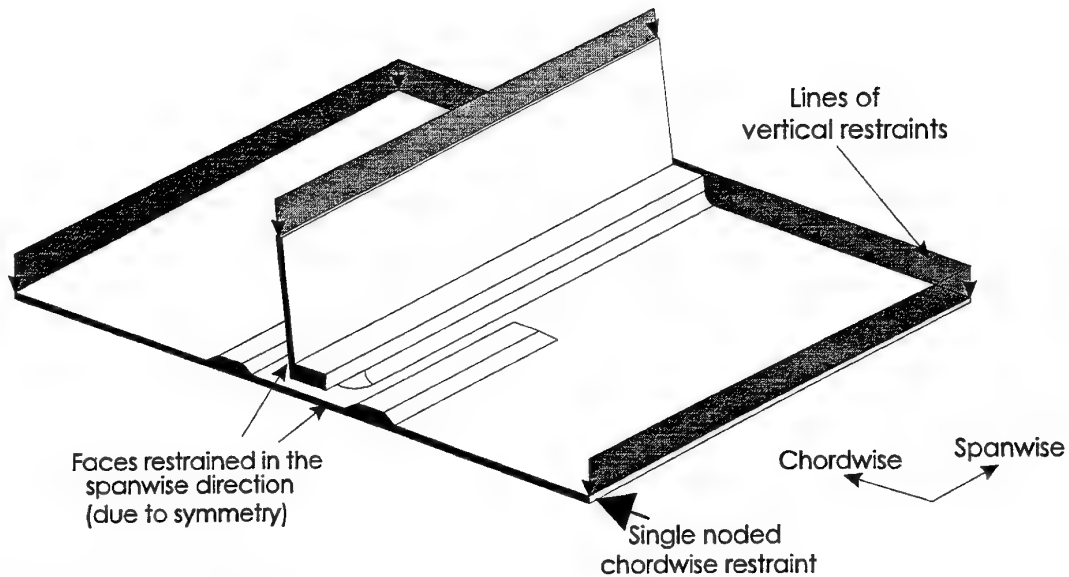
Fig 11. Location of restraints

4.7 Loading

The loading of the FE model is shown in Figure 12, including the wing skin and spar cap. The spar web was not loaded. The magnitude of the applied far-field tension loading was found from multiplying the average of the far-field rosette strains from the full wing strain survey at 100% CPLT, by the Young's modulus. These calculations are found in section 3.3, the far-field applied load was determined to be 193.19 MPa

Applied far field stress
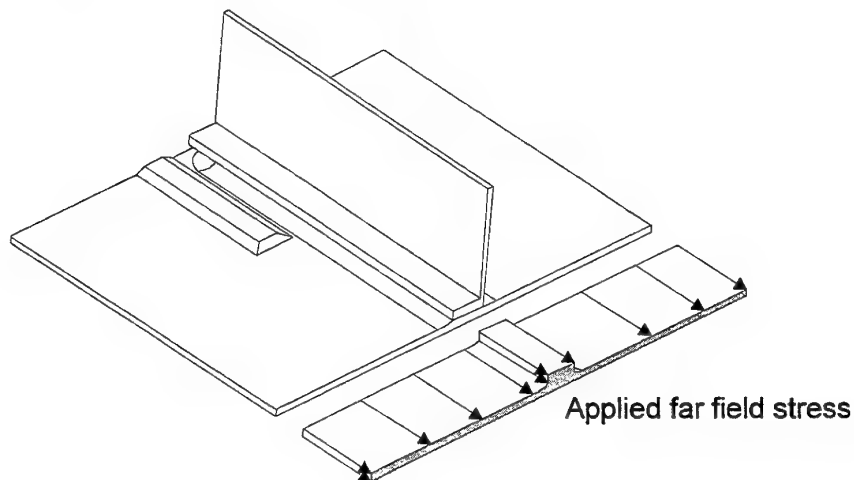
Fig 12. Location of loading

5. Validation

Validation of the FE model included the following considerations which are discussed in more detail below:

- *Convergence testing*
- *Geometric sensitivity study*
- *Strain / load comparisons (experimental / FE)*
- *Applied load selection*

5.1 Convergence

The principal strains along the chordwise symmetry line of the FE model were compared to those from a model with a coarser mesh density. Results indicated less than one percent difference in strains between the models. The small difference in magnitude indicated that numerical convergence had been achieved.

If the mesh is too coarse for the strain gradient, a large variation between the unaveraged strains would exist at any particular node within this region. Strain averaging along the triangular prism elements and several chord-wise lines were investigated. Results indicate relatively minor differences (less than an order of magnitude) between the nodal maximum and minimum unaveraged strains. This confirms adequate element size selection and suggests an appropriate element geometry for the load environment.

5.2 Geometric sensitivity

A detailed sensitivity study on the effect of small geometry changes to the FE model is reported in [3]. It was found that small changes of the radii and thickness of the wing skin can give a notable variation in the stresses and strains at the fuel-flow passage. The results presented here are for the baseline configuration of the static test wing described in Section 2.3.

5.3 Stress / load comparison with experimental data

A comparison of material and test wing stress-strain curves with the FE results at certain locations predicts yielding within the test wing.

A comparison of the maximum principal stress on the inside wing skin surface at the centre of the FFP with the material stress-strain curves is shown below in Figure 13. Since the FE model is linear elastic, it predicts a stress at this location under 100% CPLT load of 463 Mpa. As shown in Figure 13, the material yields at 380 Mpa which corresponds to 82% of the CPLT load. This graph indicates that yielding has occurred at CPLT loading. The existence of plasticity creates a change in local material stiffness.
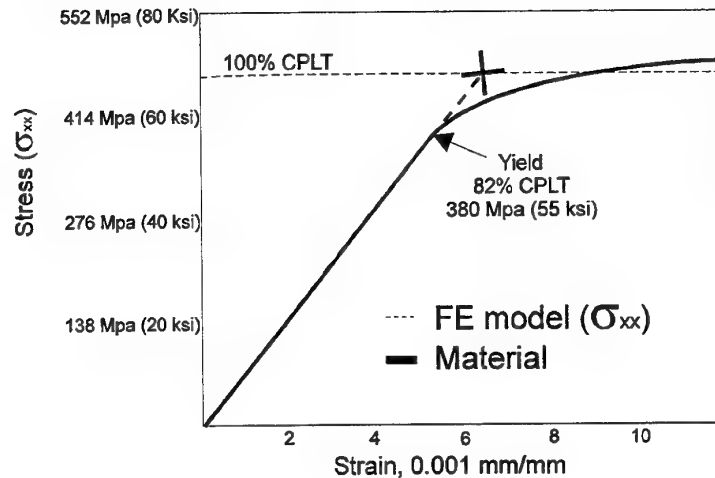

Fig 13. Unidirectional stress comparison between material properties [8] and spanwise stress from the FE model at the center of the fuel-flow passage (inside surface).

A comparison of the test wing load-strain curve with the FE model is shown in Appendix B. The test wing load-strain graph at the centre of the FFP in Appendix B.1 is linear. No material yielding at this location is suspected since the strains are considerably lower than the material yield strain. Furthermore, since the results are linear, the localised effects from the inside surface of the test wing skin have a negligible effect on the outside surface stresses and strains for this particular wing skin thickness.

The measured strain gauge data was compared with those from the FE model. Since the FE model assumed a flat wing skin surface, a correction factor for the actual wing curvature must be applied. Wing skin curvature has the effect of altering the distance of the wing skin from the neutral axis of the wing. Span-wise strain is proportional to the distance to the neutral axis. The derivation of the correction equation can found in Appendix C.

The application of the correction equation to the returned FE strain data at CPLT loading is shown in Appendix D.

Percentage CPLT load surface-strains plots along $X=0$ for the central strain gauge (SO6_3) and the far-field rosettes on the outside surface are compared with that of the FE model at the same location in Appendix B. Appendix B.2 indicate that the NASCE can be applied to the FE model throughout the CPLT loading sequence.

5.4 Applied load selection

The FE applied far-field load was chosen on the basis of strain gauge data collected at a chordwise distance of 124 mm from the centre of the FFP. Since the CPLT strain gauge results shown in Appendix C exhibit a close match with the FE strain results, the selected FE applied stress for CPLT loading is valid.

6. Discussion

Several limitations apply to the use and validation of the FE model as follows:

- *Constant secondary bending assumption.*

- *The FE model is only linear elastic.*

- *All strain gauge comparisons were on the outside of the wing skin.*

- *All residual stresses and strains are ignored.*

- *The geometry of the inside surface of the wing can only be approximated (addressed in the sensitivity study [3])*

These items are addressed in this section.

6.1 Constant secondary bending assumption

The fuel-flow passage stress concentration is due to the coupling of secondary bending with tensile loading.

$\sigma = F/A + My/I$
$M = F.d,$

where the secondary bending term is proportional to the distance between the neutral axis of the wing skin and that of the spar landing, 'd'. As the wing skin deforms out of plane under tensile loading, the neutral axes converge. This effectively decreases the magnitude of the bending moment and consequently the total stress. The linear FE model conservatively assumes a constant neutral axis offset distance. After the test wing has deformed, the magnitude of 'd' decreases. Hence the FE assumption of a

constant linear bending moment is conservative, since it results in a higher combined stress.

6.2 Plasticity

The FE model revealed that the principal stress in the spanwise direction at the centre of the fuel-flow passage exceeded the material yield stress for CPLT loading (see Figure 12). Since it was established that the test wing had undergone a minimum of two CPLT loadings prior to the strain survey, a residual stress created by the presence of the plastic zone would most likely be present in the test wing.

CPLT testing of representative wing skin specimens of nominal skin thickness of 3.7 mm has indicated the presence of plasticity at the crack initiation site [11]. After several CPLT cycles the plastic zone size increased. The plasticity causes a localised stress redistribution. This stress redistribution resulted in lower strains being measured on the outside wing skin surface directly opposite the fuel-flow passage.

Referring again to Figure 13 since the stresses are higher in the FE model than for a yielded wing skin, the assumption of a linear FE model is conservative.

6.3 Strain gauge locations

Since it was not physically possible to access the inside surface of the test wing so as to place strain gauges, no knowledge of the strain field is available there. Testing of thinner coupons however, wherein access to the representative inside surface was available, indicates a large tension field at the centre of the FFP [11]. Due to the difference in geometry, the magnitude of the strain values are not comparable. Because of the yielding of the test wing, the stress on the inside surface of the elastic FE model would be higher than that of the specimen wing. Hence the FE models' calculation of the stresses is conservative.

6.4 Residual effects

Evidence from CPLT cycling of panel specimens has shown evidence of a residual deformation at the point of crack initiation after cycling [11]. The present FE model does not model this effect. Since the strain gauges were applied after the wing had experienced at least two CPLT cycles in its life, no residual strains could be measured. The magnitude of the residual strains is dependent upon the amount of plastic and geometric deformation. Since the residual strains are estimated to be in compression, neglecting these effects is conservative.

7. Conclusion

The far-field applied stress at CPLT loading at FASS 281.28, assuming a 4.19 mm wing skin thickness for the tested wing was calculated from the strain survey results to be 193.19 MPa (28 ksi). Under this loading the FE model produced a strain distribution which was consistent with the test wing strain survey results.

The base FE model adequately models the specimen F-111 wing skin before yielding occurs.

Yielding was found to occur on the inside surface of the fuel-flow passage at approximately 80 percent of CPLT loading. Once yielding has occurred the FE model stress and strains at this location are assumed to diverge from those of the actual wing. Strains on the outside surface after yielding continue to give adequate correlation after yielding has occurred.

Despite the localised errors that may occur due to plasticity, the overall behaviour of the model reflects the actual wing very well. Extension of the model to include a crack, and then the boron-epoxy repair patch is therefore considered feasible. This will enable quantification of important factors such as stress in the patch, shear strain in the adhesive, stress intensity reduction and thermal effects.

8. Acknowledgments

9. References

[1] WATTERS, K (1994) *F-111 Outer Wing Skin Strain Survey at Fuel Flow Hole in Forward Auxiliary Spar.* AMRL Structures laboratory Report No. 1/94, B2/03/101.

[2] McHENRY, H & KEY, R (1994) *The F-111 Logic, Familiar Materials; proven processes.* Metal Progress, p62.

[3] KEELEY, D.W, CALLINAN, R.J. & SANDERSON, S (1995) *Sensitivity study of the AMRL Finite Element model of the F-111 wing skin structural detail at Forward Auxiliary Spar Station (FASS) 281.281.* AMRL technical report.

[4] MORTON, H (1994) *DAFA NDI Report.* NDI/HM/3/94 AMRL.

[5] PENHALL, P (4/5/1995) *RE: F-111C Wing SRO#2 & FFVH-13 surveying* SES/52/5/1/02 minute. F-111 Bonded repair task. AMRL

[6] GENERAL DYNAMICS REPORT FSZ-12-360A *Test loads and General Test Procedures for F-111 Proof Testing Phase III Structural Inspection Program F-111 A/E/D/F/FB-111A, November 1985*

[7] CALLINAN, R.J. SANDERSON, S. & KEELEY, D.W (9/1994) *FE validation working file.* SES/52/12/001

[8] MIL-HDBK-5F (1/11/90) table 3.2.0.(d)

[9] SANDERSON, S., CALLINAN, R., *Development of a Data Generation Program for the Lower Wing Skin Repair of an F-111,* AMRL Technical Note, in preparation

[10] GENERAL DYNAMICS DRAWING 12W951

[11] BOYKETT,R (1995) *Detailed Strain Survey of Panel Test Specimen Representing F-111c Lower wing Skin at FASS 281* Structures Laboratory Report No 5/95

[12] WILKIN, F/L M. (1994) *Design Approval Package for the Interim Repair of F-111C Wing FAS A15-5,* Annex E, RAAF ASI/4080/14-12.

[13] GENERAL DYNAMICS REPORT FSZ-12-100 *Wing Box Design Load Conditions,* GD Convair

Appendix A

Calculation of design CPLT stress at FASS 281.28

The following method of calculating CPLT at FASS 281.28 follows that of F/L Wilkin's [12] except that the reference coordinate system has been changed from the centre spar to the Forward Auxiliary Spar (FAS) coordinate system. This change allows a direct comparison between theoretical and applied loads to the FAS.

The FASS 281.28 was found to be 208.37 mm along the 26% chord line measured from the wing pivot [7].

A CAD drawing of the wing was produced [10]. The 26% chord line coordinates were converted directly to FAS coordinates as shown below.
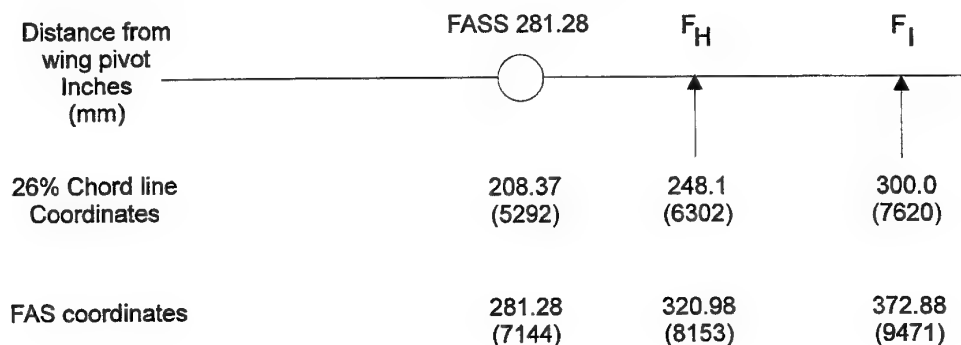
Distance from wing pivot Inches (mm)	FASS 281.28	F_H	F_I
26% Chord line Coordinates	208.37 (5292)	248.1 (6302)	300.0 (7620)
FAS coordinates	281.28 (7144)	320.98 (8153)	372.88 (9471)

Fig A1. Location of outboard wing jacks with respect to the wing pivot.

From the FAS coordinate system the local bending moment (with respect to the FASS coordinate system) from the CPLT loading can be calculated.

$$BM_{FAS\,281} = 4\,900 \times (372.88 - 281.28) + 29200 \times (320.98 - 281.28) \qquad A1$$
$$= 1\,608\,000 \text{ lb.in}$$

In 1966 GD Convair undertook 6.5g manoeuvres load analysis of the F-111A & B wing [6]. From these tests a ratio of nominal stress to wing pivot bending moment can be found. Since in this case local, stress is directly proportional to local bending moment, this ratio can be used in conjunction with the CPLT bending moment to find the local nominal stress under CPLT.

FASS 281.28 was converted to a centre spar coordinate of CSS 277.51 by directly reading from the CAD drawing of the wing.

19

This coordinate was used to determine the local bending moment ($BM_{FASS\ 281}$) from GD Convair data (Figure 3 of reference 6). The local bending moment at 6.5g loading was found to be 1.83 Mips.

For the particular flight case analysed, the nominal stress at this location was found to be 34.6 ksi (table 30, reference 6).

Hence:

$$\sigma_{FASS\ 281} / M_{FASS\ 281} = 34.6 \times 10^3 / 1.83 \times 10^3 \qquad\qquad A2$$
$$= 0.0189\ in^{-3}$$

Multiplying by the local bending moment under CPLT conditions gives the stress under CPLT conditions as follows

$$\sigma_{FASS\ 281} = 0.01883 \times 1608 \times 10^6$$
$$= 30\ 400\ psi\ (\ 209.4\ MPa) \qquad\qquad A3$$

Appendix B

Stress strain correlation

Figure B.1
Strain - Location Comparison
(Outside Surface at CPLT loading)

Onset of plasticity on the inside surface
(predicted from FE)

FE results

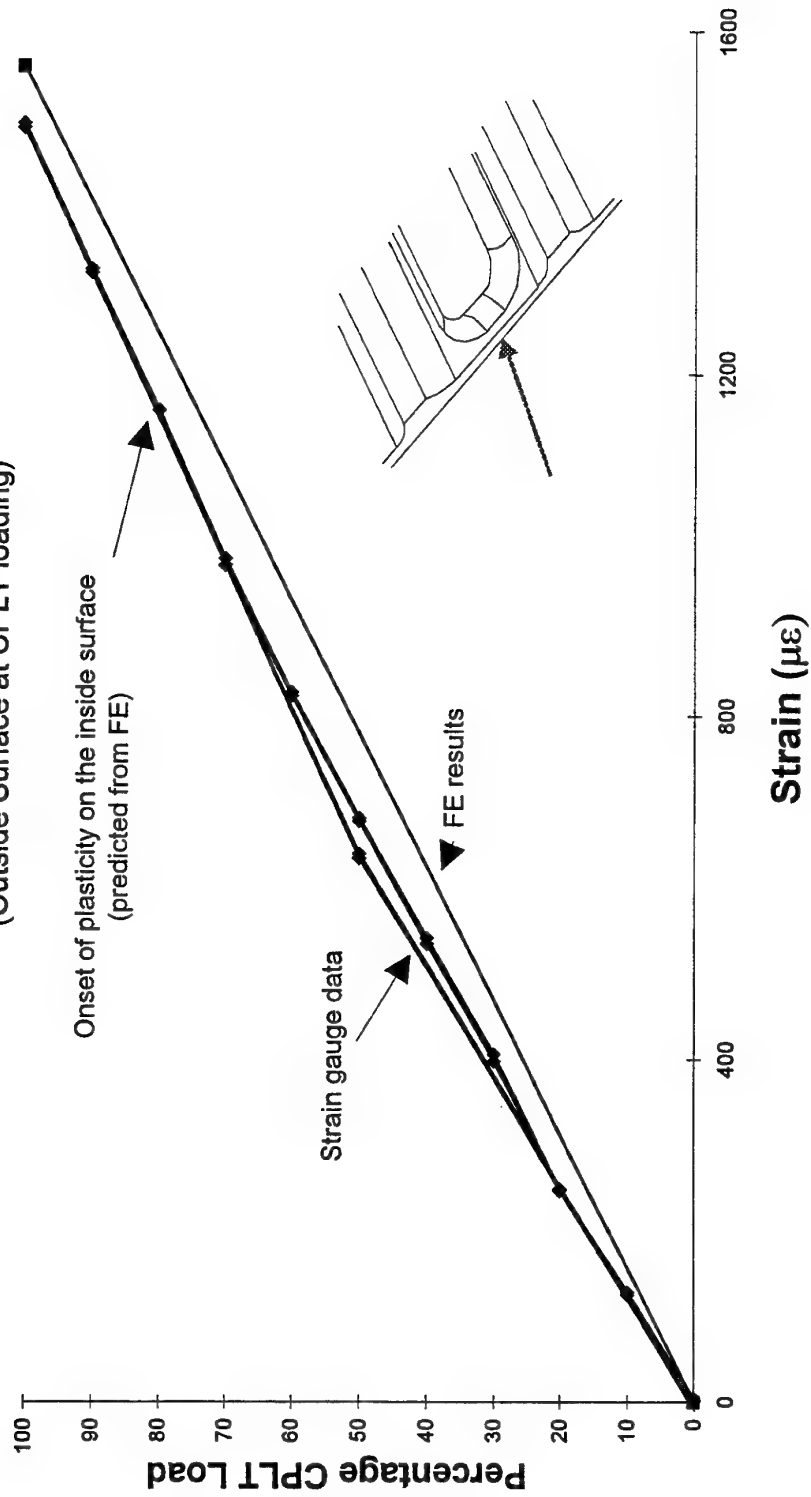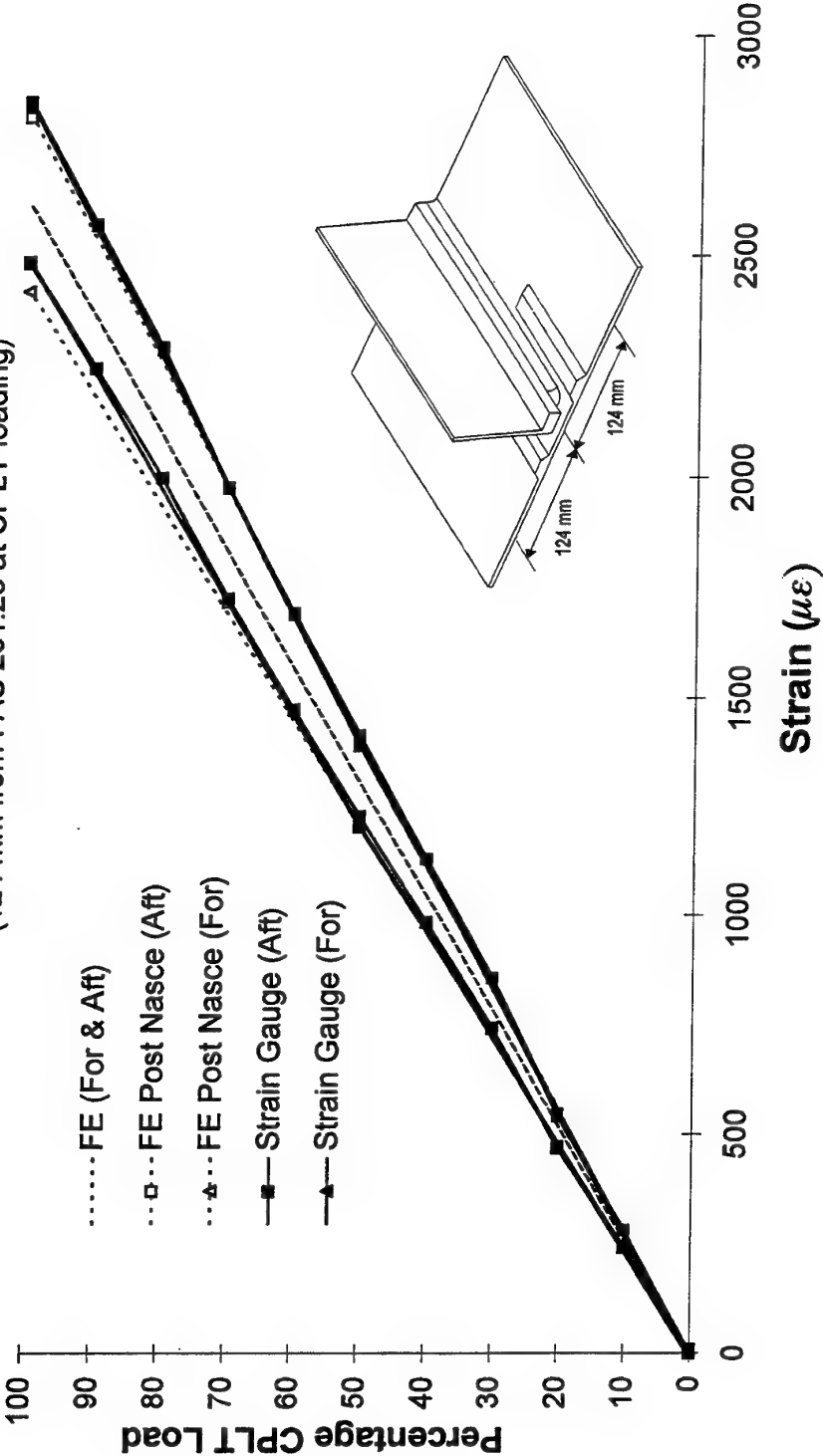Strain gauge data

Strain (με)

Percentage CPLT Load

Figure B.2
Strain - Location Comparison
(124 mm from FAS 281.28 at CPLT loading)

Appendix C

Calculation of NASCE

Consider a flat plate as shown below in Figure C1a. Strain in the chord-wise y direction is assumed to be proportional to $\bar{z}$, the distance to the neutral axis.
ie,

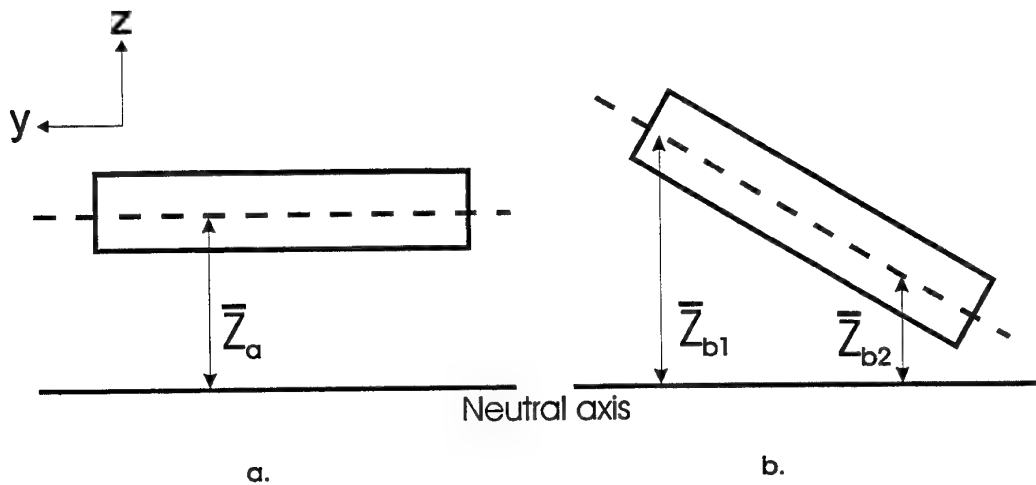$$\varepsilon_x \propto \bar{z}. \qquad\qquad C1$$

Fig C1. a. Flat plate   b. Plate with angle

For a curved wing skin $\bar{z}$ is not constant, but a function of the chord-wise y coordinate.

$$\bar{z} = f(y) \qquad\qquad C2$$

The cambered wing skin at FASS 281.28 can be approximated ideally as a linear function of y over a distance of 300 mm as shown by Figure C1b. Measurements of the slope from the actual wing approximated the slope as 1:18.

$$\bar{z} = y/18 + b \qquad\qquad C3$$
$$\varepsilon_x = c(y/18 + b) \qquad\qquad C4$$

In the strain-location plot shown below by Figure C2, the value of 'b' represents the strain axis intercept at y=0. An average of the four far-field strain gauge data at y = ±149 mm from the FAS centreline gives:

At y = 0.0, ε_x = 2740 µε.   C5
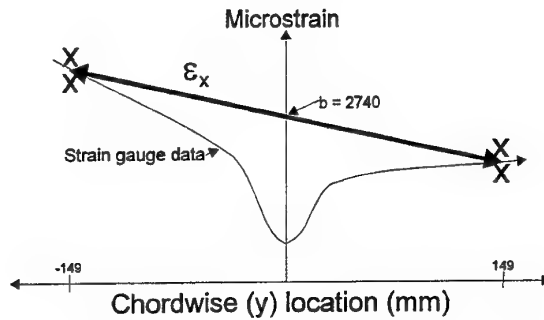

Fig C2. Spanwise strain as a function of chordwise location at FASS 281.28

Substituting this strain value for that of 'b' in equation C4 allows the proportionality constant to be calculated as:

c = 28.72 µε/mm   C6

An approximate equation for ε_x with respect to y for a flat plate with the same slope as the F-111A wing in the strain gauged area becomes:

ε_x = 1.596y + 2740 µε   C7

The correction term ($\Delta\varepsilon$) for a variation in distance from the wing-box neutral axis can therefore be expressed as follows:

$\Delta\varepsilon$ = 2740 - ε_x (y=0)   C8
       = -1.596y µε

Hence, to correct the FE results, the equation becomes:

NASCE = Fe_{actual} + correction   C9
        = Fe_{actual} -1.596y µε

Appendix D

Strain-location correlation

Figure D.1
Strain - Location Comparison
At CPLT conditions
Outside surface along chordwise symmetry line

◇ Strain Gauge run 1
□ Strain Gauge run 2
—— Original FE
—·—·— Post NASCE

Strain (με)

Chord-wise location (mm)
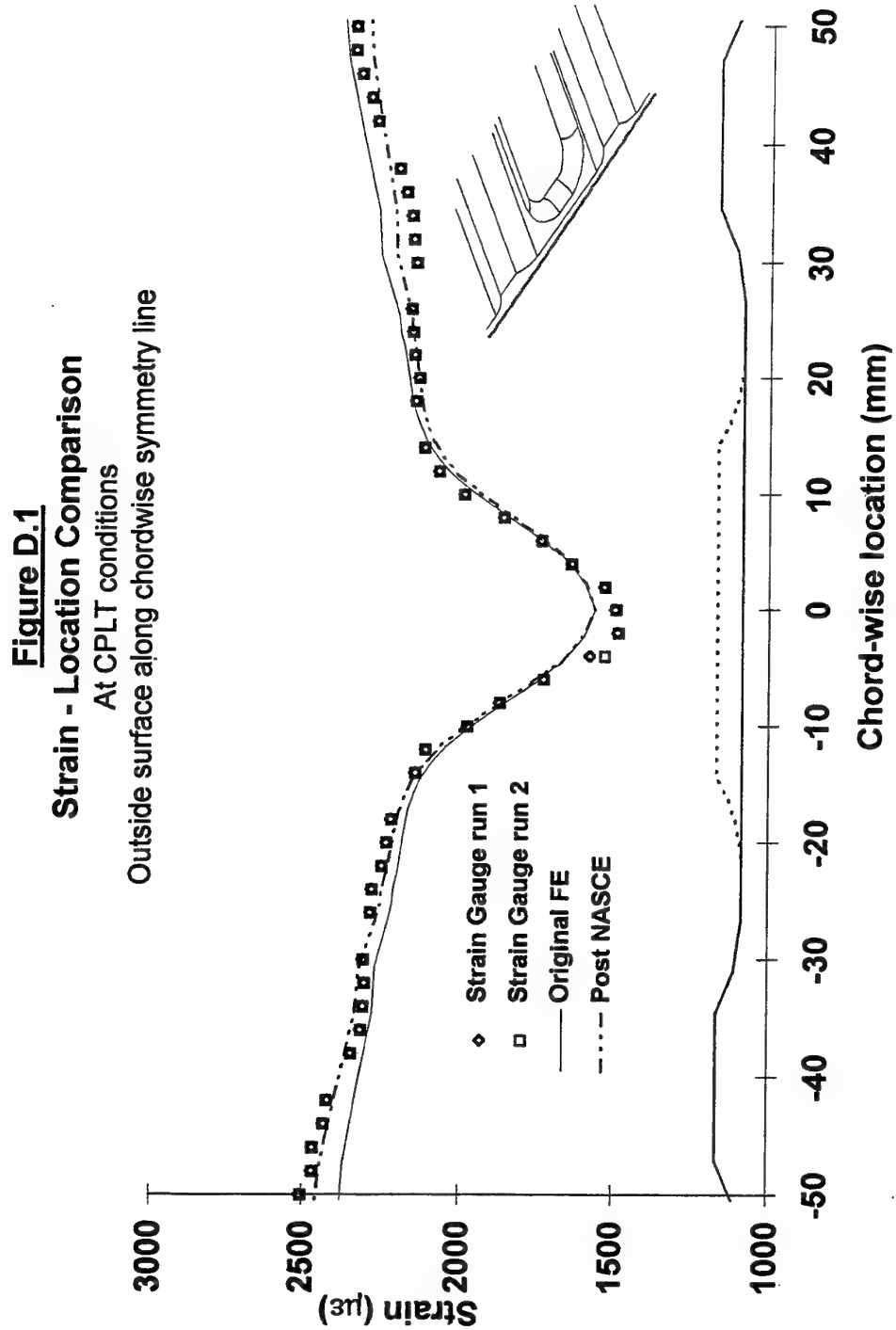
Figure D.2
Strain - Location Comparison
At CPLT conditions
Outside surface along chordwise symmetry line

◇ Strain Gauge run 1
□ Strain Gauge run 2
—— Original FE
—·—·— Post NASCE

Chord-wise location (mm)

Strain (µε)
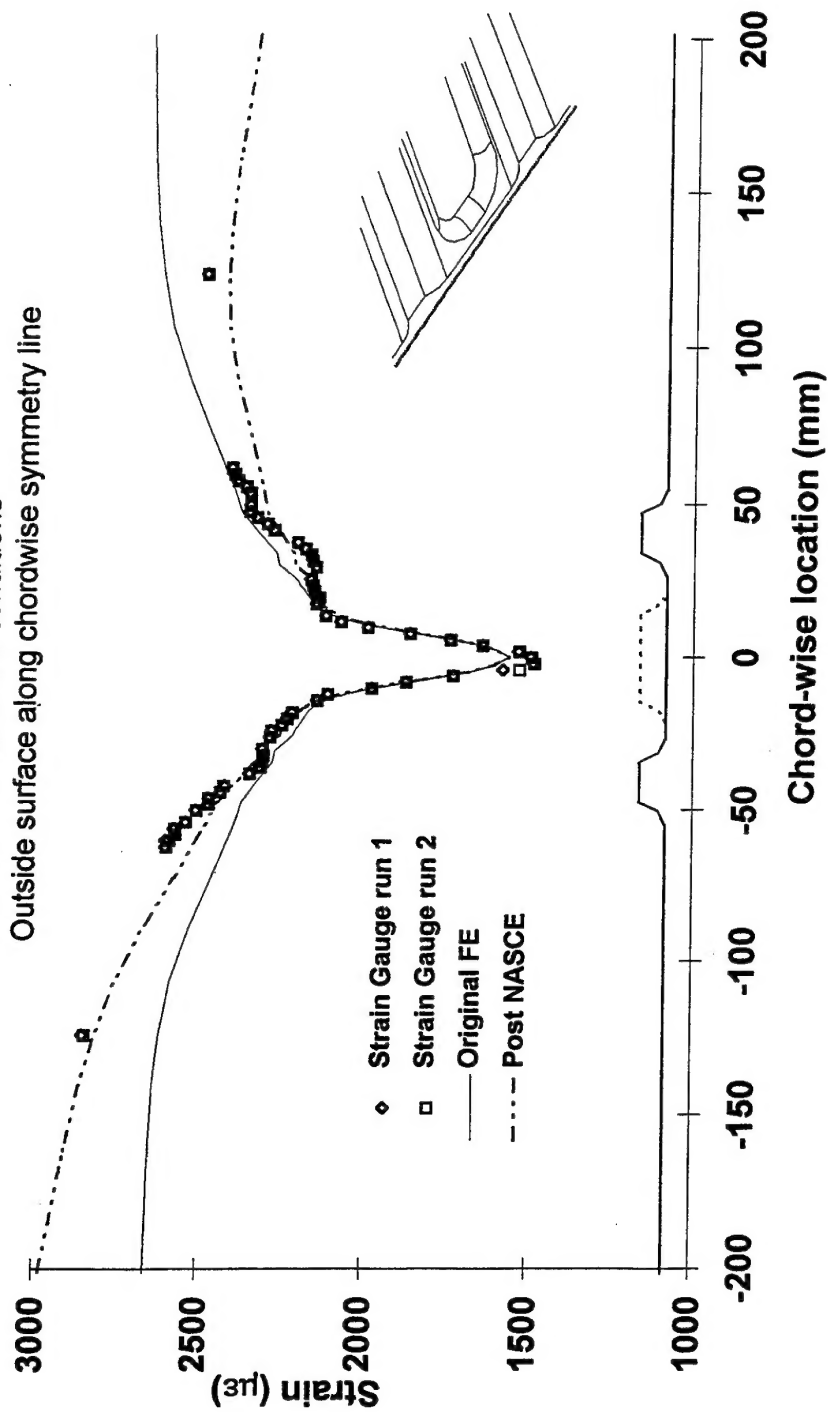
DISTRIBUTION LIST

A Validated Finite Element Model of an F-111 Lower Wing Skin Structural Detail at Forward Auxillary Spar Station (FASS) 281.28

D. Keeley, R. Callinan and S. Sanderson

AUSTRALIA

TASK SPONSOR: DTA (RAAF HQLC)

DEFENCE ORGANISATION

Defence Science and Technology Organisation

Chief Defence Scientist ⎫
FAS Science Policy ⎬ shared copy
AS Science Industry and External Relations ⎪
AS Science Corporate Management ⎭
Counsellor Defence Science, London (Doc Data Sheet only)
Counsellor Defence Science, Washington (Doc Data Sheet only)
Scientific Adviser to Thailand MRD (Doc Data Sheet only)
Senior Defence Scientific Adviser/ScientificAdviser Policy and Command (shared copy)
Navy Scientific Adviser (3 copies Doc Data Sheet and one copy distribution list)
Scientific Adviser - Army (Doc Data Sheet and distribution list only)
Air Force Scientific Adviser
Director Trials

Aeronautical and Maritime Research Laboratory

Director
Chief of Airframes and Engines Division
Research Leader
Task Manager
D. Keeley
R. Callinan
S. Sanderson

Electronics and Surveillance Research Laboratory

Director

DSTO Library

Library Fishermens Bend
Library Maribyrnong
Main Library DSTOS (2 copies)
Library, MOD, Pyrmont (Doc Data sheet only)

Defence Central

OIC TRS, Defence Central Library
Officer in Charge, Document Exchange Centre (DEC), 1 copy
DEC requires the following copies of public release reports to meet exchange
agreements under their management:
*US Defence Technical Information Centre, 2 copies
*UK Defence Research Information Centre, 2 copies

*UK Defence Research Information Centre, 2 copies
*Canada Defence Scientific Information Service, 1 copy
*NZ Defence Information Centre, 1 copy
National Library of Australia, 1 copy
Defence Intelligence Organisation
Library, Defence Signals Directorate (Doc Data Sheet only)

Air Force

Director General Force Development (Air)
OIC ATF ATS, RAAFSTT, WAGGA (2 copies)
Wing Commander E, Wilson, OIC ASI, HQLC, RAAF Williams, Laverton VIC
Flight Lieutenant S. White, SRLMSQN, RAAF Amberley, QLD
Mr M. Davis ATS1A, 501 Wing, RAAF Amberley, QLD

Army

Director General Force Development (Land) (Doc Data Sheet only)
ABCA Office, G-1-34, Russell Offices, Canberra (4 copies)

Navy

Director General Force Development (Sea) (Doc Data Sheet only)

UNIVERSITIES AND COLLEGES

Australian Defence Force Academy
    Library
    Head of Aerospace and Mechanical Engineering
Senior Librarian, Hargrave Library, Monash University
Librarian, Flinders University

OTHER ORGANISATIONS

NASA (Canberra)
AGPS

ABSTRACTING AND INFORMATION ORGANISATIONS
INSPEC: Acquisitions Section Institution of Electrical Engineers
Library, Chemical Abstracts Reference Service
Engineering Societies Library, US
American Society for Metals
Documents Librarian, The Center for Research Libraries, US

INFORMATION EXCHANGE AGREEMENT PARTNERS
Acquisitions Unit, Science Reference and Information Service, UK
Library - Exchange Desk, National Institute of Standards and Technology, US
National Aerospace Laboratory, Japan
National Aerospace Laboratory, Netherlands

SPARES (10 copies)

Total number of copies: 61

DEFENCE SCIENCE AND TECHNOLOGY ORGANISATION DOCUMENT CONTROL DATA		1. PRIVACY MARKING/CAVEAT (OF DOCUMENT)			
2. TITLE A Validated Finite Element Model of an F-111 Lower Wing Skin Structural Detail at Forward Auxillary Spar Station (FASS) 281.28		3. SECURITY CLASSIFICATION (FOR UNCLASSIFIED REPORTS THAT ARE LIMITED RELEASE USE (L) NEXT TO DOCUMENT CLASSIFICATION) Document (U) Title (U) Abstract (U)			
4. AUTHOR(S) D. Keeley, R. Callinan and S. Sanderson		5. CORPORATE AUTHOR Aeronautical and Maritime Research Laboratory PO Box 4331 Melbourne Vic 3001			
6a. DSTO NUMBER DSTO-TN-0046	6b. AR NUMBER AR-009-759	6c. TYPE OF REPORT Technical Note		7. DOCUMENT DATE June 1996	
8. FILE NUMBER M1/9/90/1	9. TASK NUMBER AIR 94/118	10. TASK SPONSOR DTA (RAAF HQLC)	11. NO. OF PAGES 25		12. NO. OF REFERENCES 13
13. DOWNGRADING/DELIMITING INSTRUCTIONS None		14. RELEASE AUTHORITY Chief, Airframes and Engines Division			

15. SECONDARY RELEASE STATEMENT OF THIS DOCUMENT

Approved for public release

OVERSEAS ENQUIRIES OUTSIDE STATED LIMITATIONS SHOULD BE REFERRED THROUGH DOCUMENT EXCHANGE CENTRE, DIS NETWORK OFFICE, DEPT OF DEFENCE, CAMPBELL PARK OFFICES, CANBERRA ACT 2600

16. DELIBERATE ANNOUNCEMENT

No limitations

17. CASUAL ANNOUNCEMENT	Yes

18. DEFTEST DESCRIPTORS

Bonded Composite Repair; Aircraft Structural Integrity; Fatigue; Repair; Finite Element Analysis; F-111; Residual Strength

19. ABSTRACT
This report describes an AMRL developed and validated Finite Element (FE) model of the F-111A lower wing skin (Serial Number A-10-824) at Forward Auxiliary Spar Station (FASS) 281.28. and constitutes part of an extensive AMRL bonded composite repair substantiation program initiated by the RAAF following the discovery of fatigue cracking at FASS 281.28 in an F-111C aircraft. Strain data from the FE model is compared with measured strain gauge data from an F-111A static test wing under Cold Proof Loading Test (CPLT) or limit conditions. A relationship between nominal section stress at FASS 281.28 and local bending moment is established. The FE model will be further developed to include the fatigue crack, the adhesive and the boron epoxy patch.